Chemistry of Sulfur Oxides on Transition Metals I: Configurations, Energetics, Orbital Analyses, and Surface Coverage Effects of SO_2 on Pt(111)

Xi Lin

Department of Chemistry, Massachusetts Institute of Technology, Cambridge, Massachusetts 02139-4301

Kenneth C. Hass and William F. Schneider

Physical and Environmental Sciences Department, Ford Research Laboratory, MD 3083-SRL, Dearborn, Michigan 48121-2053

Bernhardt L. Trout*

Department of Chemical Engineering, Massachusetts Institute of Technology, Cambridge, Massachusetts 02139-4301

Received: May 16, 2002; In Final Form: September 23, 2002

An extensive search for stable chemisorbed SO_2 configurations on the Pt(111) surface has been performed using first-principles DFT−GGA calculations. The most energetically stable configurations, η^2-S_b,O_a and η^3-S_a,O_a,O_a at fcc sites, where η^2 and η^3 mean that the number of atoms of the adsorbate coordinated to surface atoms are two and three, respectively, and the subscripts a and b stand for the atoms on atop sites and bridge sites, respectively, are consistent with experimental observations. It is found that strong sulfur−metal bonds are essential in stabilizing the molecular SO_2 binding to the Pt(111) surface. The lateral dipole−dipole interactions among chemisorbed SO_2 moieties are shown to be responsible for the strong coverage effect of the SO_2 binding energy to the surface. These strong lateral interactions do not greatly affect the molecular structures or relative binding energy differences among different binding configurations. The projected density of states and the induced density of states are studied in detail to explain binding effects.

I. Introduction

Long known as some of the major poisoning compounds in heterogeneous catalysis, sulfur-containing molecules, such as SO_2, have highly poisonous effects on the automotive emission control of hydrocarbons, carbon oxides, and nitrogen oxides.[1,2] Moreover, the importance of sulfur chemistry on metal surfaces was recently highlighted in a series of extensive experimental studies focused on understanding how SO_2 promotes the oxidation of alkanes, such as propane.[3−5]

To understand the reactivity of sulfur-containing molecules in heterogeneous catalysis, researchers have started investigating the molecular structure of SO_2 on transition metal surfaces,[6] such as Pt(111),[3,4,7−10] Cu(111),[11−13] Cu(100),[11,14] Ni(111),[15] Ni(110),[16,17] Ni(100),[15] Rh(110),[18] Ag(110),[19] and Pd(100).[20] Insights into the binding structure of SO_2 on Pt(111) have been accumulated through experimental work in the past two decades. The difficulties in experiments are mainly due to the existence of the complex three-atom adsorbate mixed with more complicated coadsorbed decomposition and recombination products.[1]

It is generally agreed that SO_2 absorbs molecularly on Pt(111) at low temperatures, typically 100−160 K. Through XPS, UPS, TPD, and HREELS, Sun et al.[9] concluded that the binding of the SO_2 molecule was via an η^2-S,O structure, where η^n means that n atoms of the adsorbate are coordinated to surface atoms and the atoms following the dash are the coordinated atoms, with the SO_2 molecular plane essentially perpendicular to the Pt(111) surface. Their simple frontier molecular orbital analysis suggested a preferred configuration with the sulfur atom on a bridge site and one oxygen atom on an atop site. More recently, Polčik et al.[10] claimed to detect a new, flat-lying configuration of SO_2 on the Pt(111) surface at 150 K in their combined XPS and NEXAFS study, and they pointed out that this flat-lying configuration was invisible in the HREELS experiments by Sun et al.[9] However, Polčik et al. did not propose any detailed structural information for this flat-lying configuration. Sellers and Shustorovich employed the empirical bond order conservation−Morse potential method[21,22] and concluded that the most stable configurations involved bicoordination binding through both η^2-S,O and η^2-O,O structures on the Pt(111) surface but no flat-lying configurations.

This study aims to investigate extensively possible configurations of SO_2 on Pt(111) at varying coverages. We report energetic and structural results of 20 different stable and metastable configurations. Furthermore, our results tend to confirm the experimental results discussed above, i.e., the presence of the η^2-S,O species (perpendicular to the surface) and the η^3-S,O,O species (flat-lying on the surface). However, all of the possible η^2-O,O configurations were found to be weakly bound at $^1/_9$ ML and lower coverages, where the convention of 1 ML coverage is used to represent the full coverage of the surface, i.e., one adsorbate molecule per surface metal atom. Furthermore, the projected density of states (pDOS) on the atomic basis sets and the induced density of states (iDOS), defined as the difference in the density of states between the adsorbate−

* To whom all correspondence should be addressed. Electronic mail: trout@mit.edu.

10.1021/jp026128f CCC: $22.00
Published on Web 11/12/2002

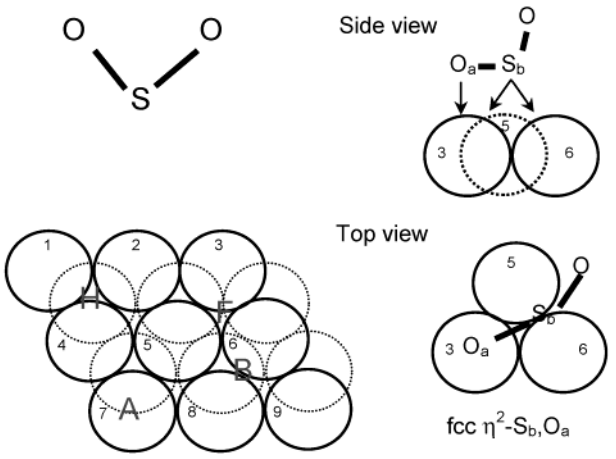

Figure 1. Schematic representation of isolated SO_2, the clean surface, and the most stable binding configuration.

substrate and the bare substrate surface, are analyzed in detail to interpret the bindings.

II. Nomenclature and Computational Details

Because of the existence of various complicated chemisorption configurations of the molecular adsorbates on the surface, a special nomenclature is introduced to categorize these configurations. The nomenclature rules are described below through examples.

For instance, the most strongly bound configuration is named fcc η^2-S_b,O_a (refer to Figures 1 and 2a). The term fcc means that the molecule is primarily adsorbed above a three-fold fcc hollow site, such as that formed by atoms number 3, 5, and 6 sketched in Figure 1. η^2 indicates that two adsorbate atoms are simultaneously bound to the substrate, and the explicit atoms are marked after the dashed line, i.e., sulfur and oxygen atoms in this case. The subscripts of the atoms represent their actual locations on the surface, such that a represents an atop site, b a bridge site, f a face-centered-cubic (fcc) three-fold site, and h a hexagonal close-packed (hcp) three-fold site. In Figure 1, the lack of a subscript on the oxygen atom indicates that this oxygen atom is not directly coordinated to the surface. Another example is bridge η^2-O,O || (refer to Figure 2i). The term bridge means that the molecule is primarily over a bridge site. || shows that the plane of the adsorbate molecule is parallel to the line connecting the two metal atoms that form the bridge. Alternatively, $\perp$ is used when the plane of the adsorbate molecule is perpendicular to the bridge. (Refer to Figure 2b.) When further distinction is required, parentheses will be introduced in the nomenclature to label the adsorbate atoms that are not directly bound to the surface, such as atop η^1-S_a(O_b,O_b) (refer to Figure 2e) and atop η^1-S_a(O_f,O_h). The former adsorbate molecule has two oxygen atoms located primarily above two bridge sites, whereas the latter adsorbate molecule has two oxygen atoms located primarily above an fcc site and an hcp site. Note that none of the oxygen atoms listed (in parentheses) are directly coordinated to the metal surface atoms.

The GNU publicly licensed software DACAPO[23] was used in this study. Slab models with the periodic boundary along the surface plane were used to simulate the Pt(111) surface. A three-layer slab model was used for the main calculations, and a four-layer model was used to check the convergence in binding structures and energetics. Specifically, calculations of the most stable configuration of SO_2 without and with one additional oxygen atom coadsorbate were performed on both three- and four-layer slabs. The bond length differences were less than 0.01 Å, and the binding energies decreased by only 1−8 kJ/mol when the fourth layer was included. In all of the models, the atoms of the bottom layer were fixed at a lattice constant of $a = 4.00$ Å. (This value is the calculated bulk lattice constant of our model and is very close to the experimental value of $a = 3.92$ Å.) The p(2 × 2) lateral supercell was used to sample comprehensively the chemisorption configurations, and the p(3 × 3) lateral supercell was used for computation of the most energetically stable configurations at a lower surface coverage. The p(2 × 2) surface supercell contains four Pt atoms per layer with a lateral lattice constant of 5.66 Å. The p(3 × 3) surface supercell has nine Pt atoms per layer with a lateral lattice constant of 8.49 Å. After the identification of the most energetically stable configuration, a few calculations of this configuration were performed for the $(\sqrt{3} \times \sqrt{3})$R30°, $(\sqrt{7} \times \sqrt{7})$R19°, $(\sqrt{13} \times \sqrt{13})$R14°, and p(4 × 4) supercells to exam the trend of the lateral interactions.

A vacuum of ∼10 Å was placed above the slabs, and one additional external dipole layer was generated self-consistently in the middle of the vacuum regions. This is necessary because strong dipoles frequently form upon adsorption of the SO_2 species. The self-consistent external dipole layer was located toward the middle of the vacuum at the minimum in the electronic density.[24] The perpendicular dipole moment of the slab was calculated by integrating the product of the charge density and the *z* component of the real-space coordinates along the *z* direction, which was set to the direction perpendicular to the metal surface in our calculations. Furthermore, by decoupling the dipole interactions among an infinite number of slabs, one is able to obtain absolutely convergent dipole−dipole interaction energies on the 2-D metal surface, instead of having conditional convergence in 3-D space.[25]

The core electrons of all atoms were treated via ultrasoft pseudopotentials[26,27] with an energy cutoff of 25 Ry for both electronic wave function and density. A higher-energy cutoff of 30 Ry was used to check the convergence. The d-channel was included explicitly for a more accurate treatment of the sulfur core.[28] The PW91[29] gradient-corrected exchange-correlation functional was used in the self-consistent DFT calculations. The geometry optimization was performed using a 4 × 4 × 1 Monkhorst−Pack[30] *k*-point mesh for the p(2 × 2), $(\sqrt{7} \times \sqrt{7})$R19°, and p(3 × 3) supercells, and the convergence with respect to *k*-points had been comfirmed.[28] A 6 × 6 × 1 Monkhorst−Pack *k*-point mesh was used for the $(\sqrt{3} \times \sqrt{3})$R30° supercell calculations, and a 2 × 2 × 1 Monkhorst−Pack *k*-point mesh was used for the $(\sqrt{3} \times \sqrt{3})$R14° and p(4 × 4) calculations. To accelerate the convergence, a 0.2 eV electronic temperature was introduced to sample the bands in reciprocal space, and the energy was extrapolated to 0 K. Because of the natural paired electron occupancies of the adsorbates, spin polarization effects were not considered to be important and therefore were not treated explicitly in the study.

III. Results and Discussion

The binding energetics and geometric data of dozens of stable configurations, i.e., local minima on the adiabatic potential surface, are presented in Tables 1 and 2, respectively. A few representative configurations are plotted in Figure 2.

A. Strength of Binding and Structural Analysis. As shown in Table 1, the binding strength of the 20 stable Pt(111)−p(2 × 2)−SO_2 configurations can be categorized into three major groups: strongly bound, intermediately bound, and weakly bound.

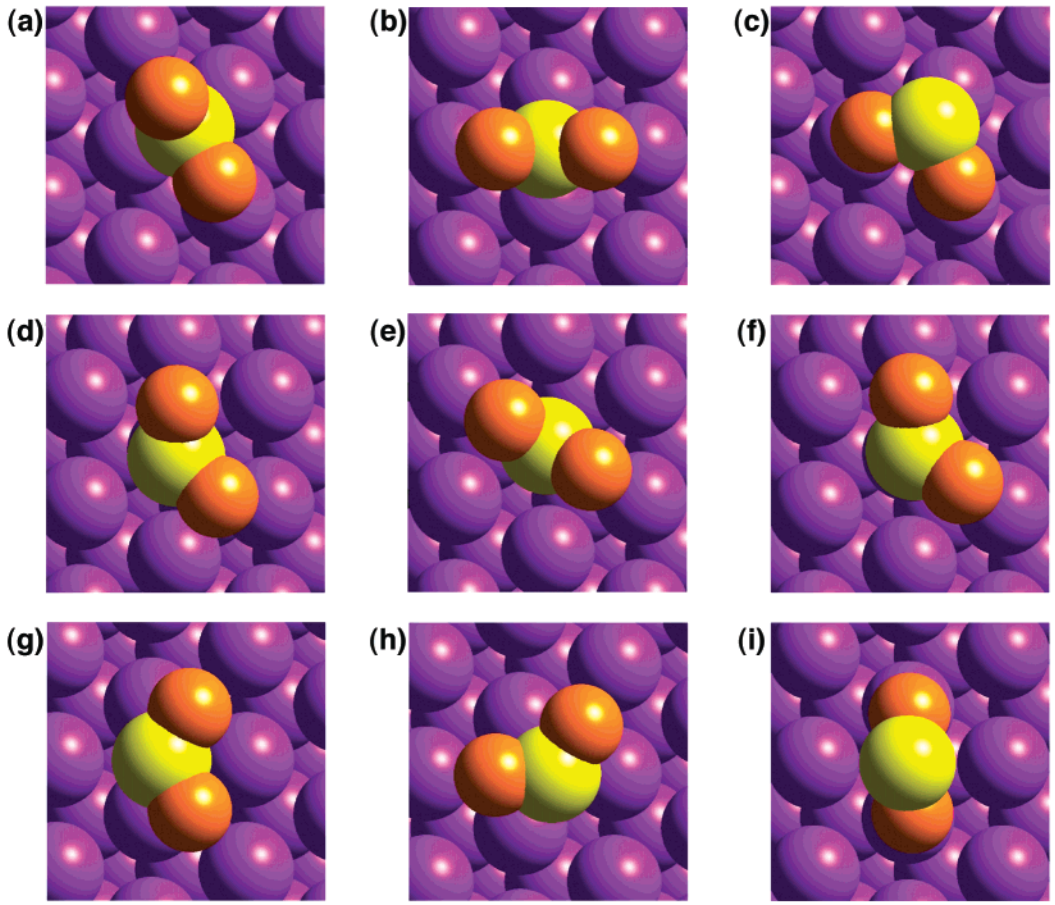

Figure 2. Top views of different binding configurations of SO_2 on the Pt(111) surface: (a) fcc η^2-S_b,O_a, (b) bridge η^1-S $\perp$, (c) fcc η^3-S_a,O_a,O_a, (d) hcp η^2-S_a,O_b, (e) atop η^1-S_a(O_b,O_b), (f) atop η^3-S_a,O_b,O_b, (g) hcp η^3-S_b,O_b,O_b, (h) η^3-S_h,O_f,O_f, and (i) bridge η^2-O,O $\parallel$. Note that certain atoms that might be pictured because of the periodic boundary conditions have been removed for clarity.

TABLE 1: Twenty Stable Binding Configurations of SO_2 on Pt(111)

configuration	figure index	molecular plane orientation	z-axis dipole moment (D) p(2 × 2)	z-axis dipole moment (D) p(3 × 3)	binding energy (kJ/mol) p(2 × 2)	binding energy (kJ/mol) p(3 × 3)
strong binding						
fcc η^2-S_b,O_a	2a	$\perp$	−0.77	−1.17	97.68	117.57
hcp η^2-S_b,O_a		$\perp$	−0.83	−1.17	88.88	107.02
bridge η^1-S $\perp$	2b	$\perp$	−0.96	−1.43	90.69	105.13
fcc η^3-S_a,O_a,O_a	2c	$\parallel$	0.02	−0.07	89.29	107.18
hcp η^3-S_a,O_a,O_a		$\parallel$	0.03	−0.07	88.57	102.80
intermediate binding						
fcc η^2-S_a,O_b		∠ 57.7°	−0.70		48.28	
hcp η^2-S_a,O_b	2d	∠ 43.2°	−0.75		47.17	
atop η^1-S_a(O_b,O_b)	2e	$\perp$	−0.30		45.34	
atop η^1-S_a(O_f,O_h)		$\perp$	−0.30		47.37	
atop η^3-S_a,O_b,O_b	2f	∠ 35.2°	−0.66	−1.07	50.38	58.19
atop η^3-S_a,O_f,O_f		∠ 34.9°	−0.65		46.44	
atop η^3-S_a,O_h,O_h		∠ 36.4°	−0.64		46.15	
weak binding						
fcc η^3-S_b,O_b,O_b		$\parallel$	0.28		14.34	
hcp η^3-S_b,O_b,O_b	2g	∠ 20.9°	0.18		12.63	
η^3-S_f,O_h,O_h		$\parallel$	0.17		13.74	
η^3-S_h,O_f,O_f	2h	$\parallel$	0.26		12.75	
bridge η^2-O,O $\perp$		$\perp$	2.20		−20.14	
bridge η^2-O,O	2i	$\perp$	1.76	1.62	−11.70	7.29
atop η^2-O_b,O_b		$\perp$	2.36		−30.66	
atop η^2-O_f,O_h		$\perp$	2.30		−26.16	

The configurations in the strongly bound group can be placed in two distinct categories. The first category consists of the most energetically stable configuration, fcc η^2-S_b,O_a (Figure 2a), hcp η^2-S_b,O_a, and bridge η^1-S $\perp$ (Figure 2b). These three configurations have a sulfur at a bridge site and a molecular plane perpendicular to the metal surface. The fact that these are the most energetically stable configurations is consistent with the results of XPS, UPS, TPD, and HREELS experiments by Sun et al.[9] A binding energy between 93.5 and 129.6 kJ/mol, depending on the surface coverage, is obtained for the most energetically stable configuration, fcc η^2-S_b,O_a (refer to section III.C for details on the range of binding energies). This range of binding energies is similar to the range presented by a temperature-programmed desorption (TPD) study, which suggested a broad range from 100 to 150 kJ/mol.[7] To our knowledge, no more accurate energetic data on this system have been reported.

The other category consists of two configurations, fcc η^3-S_a,O_a,O_a (Figure 2c) and hcp η^3-S_a,O_a,O_a, both of which have three adsorbate atoms, each located on the top of one Pt atom at a three-fold site. The molecular plane is parallel to the metal surface. We believe that one or both of these arrangements were detected as the flat-lying configuration reported by Polčik et al.[10] in their combined XPS and NEXAFS experiments.

By studying the weakly bound group of configurations, one notices that any sharing of surface metal atoms among the sulfur and two oxygen atoms makes the overall binding much weaker, for example, 88.6−89.3 kJ/mol in binding energy for η^3-S_a,O_a,O_a versus 12.6−14.3 kJ/mol in binding energy for η^3-S_b,O_b,O_b. Sharing of surface metal atoms also leads to the second type of weakly bound species, η^3-S_f,O_h,O_h and η^3-S_h,O_f,O_f (Figure 2h), with binding energies of 13.7 and 12.8 kJ/mol, respectively. There are no cases of strong binding in which surface metal atoms are shared.

TABLE 2: Binding Geometry of Pt(111)−p(2 × 2)−SO_2[a]

configuration	bond length (Å) S−O	Pt−S	Pt−O	O−S−O angle
		strong binding		
fcc η^2-S_b,O_a	1.54	2.31 (×2)	2.30	115.5°
	1.47			
hcp η^2-S_b,O_a	1.52	2.33 (×2)	2.43	116.5°
	1.47			
bridge η^1-S ⊥	1.48	2.34 (×2)	3.05	118.9°
	1.48			
fcc η^3-S_a,O_a,O_a	1.55 (×2)	2.33	2.23 (×2)	106.0°
hcp η^3-S_a,O_a,O_a	1.55 (×2)	2.34	2.24 (×2)	108.7°
		intermediate binding		
fcc η^2-S_a,O_b	1.48	2.33	3.43, 3.61	119.8°
	1.48			
hcp η^2-S_a,O_b	1.49	2.37	3.18, 3.48	119.1°
	1.48			
atop η^1-S_a(O_b,O_b)	1.47 (×2)	2.25		119.8°
atop η^1-S_a(O_f,O_h)	1.47	2.25		120.2°
	1.47			
atop η^3-S_a,O_b,O_b	1.49 (×2)	2.37	3.17, 3.25 (×2)	119.0°
atop η^3-S_a,O_f,O_f	1.48 (×2)	2.37	3.17, 3.40, 3.42 (×2)	118.5°
atop η^3-S_a,O_h,O_h	1.48 (×2)	2.36	3.18, 3.41, 3.43 (×2)	118.6°
		weak binding		
fcc η^3-S_b,O_b,O_b	1.51 (×2)	2.75 (×2)	2.68, 3.13 (×2)	114.3°
hcp η^3-S_b,O_b,O_b	1.48 (×2)	3.38 (×2)	3.49, 3.87 (×2)	117.9°
η^3-S_f,O_h,O_h	1.48 (×2)	3.61	3.82, 3.83, 3.92 (×2)	118.1°
		3.61 (×2)		
η^3-S_h,O_f,O_f	1.47 (×2)	3.49	3.74, 3.78, 3.87 (×2)	118.1°
		3.50 (×2)		
bridge η^2-O,O ⊥	1.48 (×2)		3.13 (×2)	120.5°
bridge η^2-O, O	1.49 (×2)		2.69 (×2)	118.0°
atop η^2-O_b,O_b	1.48 (×2)		3.09, 3.17 (×2)	119.3°
atop η^2-O_f,O_h	1.49		3.06, 3.30, 3.30	119.6°
	1.49		3.11, 3.31, 3.31	

[a] Note that our calculated gas-phase SO_2 has a S−O bond length of 1.47 Å and a bond angle of 120° and that the dipole moments contain only the component normal to the surface.

By comparing the energetics of the strongly bound group to the energetics of the intermediately bound group, one sees that the sulfur atom prefers to be as coordinated as possible. However, the two η^3-S_a,O_a,O_a configurations are still in the strong binding group because all three of the SO_2 atoms are coordinated to Pt, without sharing Pt atoms. The preference of forming sulfur−metal bonds indicates the essential role of these sulfur−metal bonds in stabilizing the overall SO_2 molecular binding to the surface. The strong binding configurations have an energy range from 89 to 98 kJ/mol, whereas the intermediate binding configurations have only about half of that value, from 45 to 50 kJ/mol. This implies that a bicoordinated sulfur atom can effectively provide twice the binding energy of a monocoordinated sulfur atom. The weakly bound configurations, having a range of binding energies from −30.7 to −11.7 kJ/mol under a $^1/_4$ ML surface coverage, involve only oxygen−metal bonds. This again shows the importance of having sulfur−metal bonds. We notice that our conclusion on the η^2-O,O binding configuration is different from the conclusions from the empirical bond order conservation−Morse potential method,[21,22] in which Seller and Shustorovich found configurations of η^2-O,O that are as stable as the most stable η^2-S,O binding configurations.

Note that, as the coverage decreases, as shown in Table 1, the binding energies of the η^2-O,O binding configuration become positive. For example, the bridge η^2-O,O. configuration (Figure 2i) has binding energies of 7.3 and −11.7 kJ/mol at $^1/_9$ and $^1/_4$ ML coverages, respectively (Table 1). We believe that the negative binding energies of these η^2-O,O configurations are a consequence of unfavorable lateral interaction energies. By applying the energy-dipole rule (to be discussed in section III.C below) one can estimate a binding energy of ∼14.6 kJ/mol at the zero coverage limit for the bridge η^2-O,O. configuration.

One can further interpret negative binding energies by recalling the reference states used. All of the binding energies reported in Table 1 have a common reference state, which is the sum of energies of the clean Pt p(2 × 2) slab (a = 5.66 Å) surface with a 10 Å vacuum region and isolated SO_2 in a large supercell, 10 Å × 10 Å × 10 Å. One could choose another reference state, that of the p(2 × 2) slab with a SO_2 molecule moved above the surface. The difference in energy of this reference state and the common reference state should be equal to the magnitude of the repulsive interaction. To compute this quantity, we performed a single-point energy calculation by elevating the SO_2 of the bridge η^2-O,O. configuration by 0.5 Å along the z axis. The energy of this system is 22.3 kJ/mol higher than that of the common reference state. This value is about equal to the magnitude of the lateral repulsion, computed as the sum of the magnitudes of the negative binding energy and the zero-coverage-limit binding energy of the model, 11.7 + 14.6 = 26.3 kJ/mol.

There are four different sites on the clean Pt(111) surface: three-fold sites, consisting of fcc and hcp sites; two-fold bridge sites; and one-fold atop sites. With no exceptions, the configurations above fcc sites are more strongly bound than the corresponding configurations above hcp sites. We believe that this is due to the natural fcc preference of the metal surface because the ground state of Pt is an fcc crystal. At one-quarter coverage, the binding energy differences between fcc and hcp sites range from 1 to 9 kJ/mol. A similar conclusion was found for the chemisorption of atomic oxygen and sulfur on the Pt(111) surface.[28]

Among all of the possible stable configurations, there are three different groups, categorized by the orientations of the SO_2 molecular plane with respect to the Pt(111) surface: perpendicular, tilted, and parallel. As indicated in Table 1, the perpendicular configurations are possible by having either the sulfur atom (Pt−S−Pt) or two oxygen atoms (Pt−O−O−Pt) at a bridge site. Parallel configurations are possible only when the three atoms of the molecular SO_2 are in similar local environments, all at atop or three-fold sites, except for the case of hcp η^3-S_b,O_b,O_b, where all of the bridge sites lack space for the S−O bonds.

It is interesting to note that the most energetically stable configurations, η^2-S_b,O_a and η^3-S_a,O_a,O_a, exhibit the largest deviation of the O−S−O bond angle from the angle of the isolated gas-phase SO_2 (refer to Table 2 for details). This can be explained by the fact that a stable adsorbate configuration on the surface implies a strong coupling of the adsorbate to the metal surface, which in turn has to destabilize the original molecular components within the adsorbate by filling some unoccupied antibonding orbitals of the adsorbate.

B. Analysis of Density of States. To obtain a qualitative view of the complex chemisorption of SO_2 on the Pt(111) surface, the density of states was analyzed in detail for the most energetically stable binding configuration. Results are reported in this section. Major points are summarized and applied to several representative configurations of different binding strengths.

Under the Kohn−Sham one-particle orbital picture, the binding of adsorbates to metal surfaces can be interpreted as a combination of orbital pair interactions. When the adsorbate has a higher electronegativity than the metal surface, which is certainly true for the chemisorption of SO_2 on Pt(111), there is a so-called forward donation of electronic charge, wherein the filled bands of the metal interact with the unoccupied states of

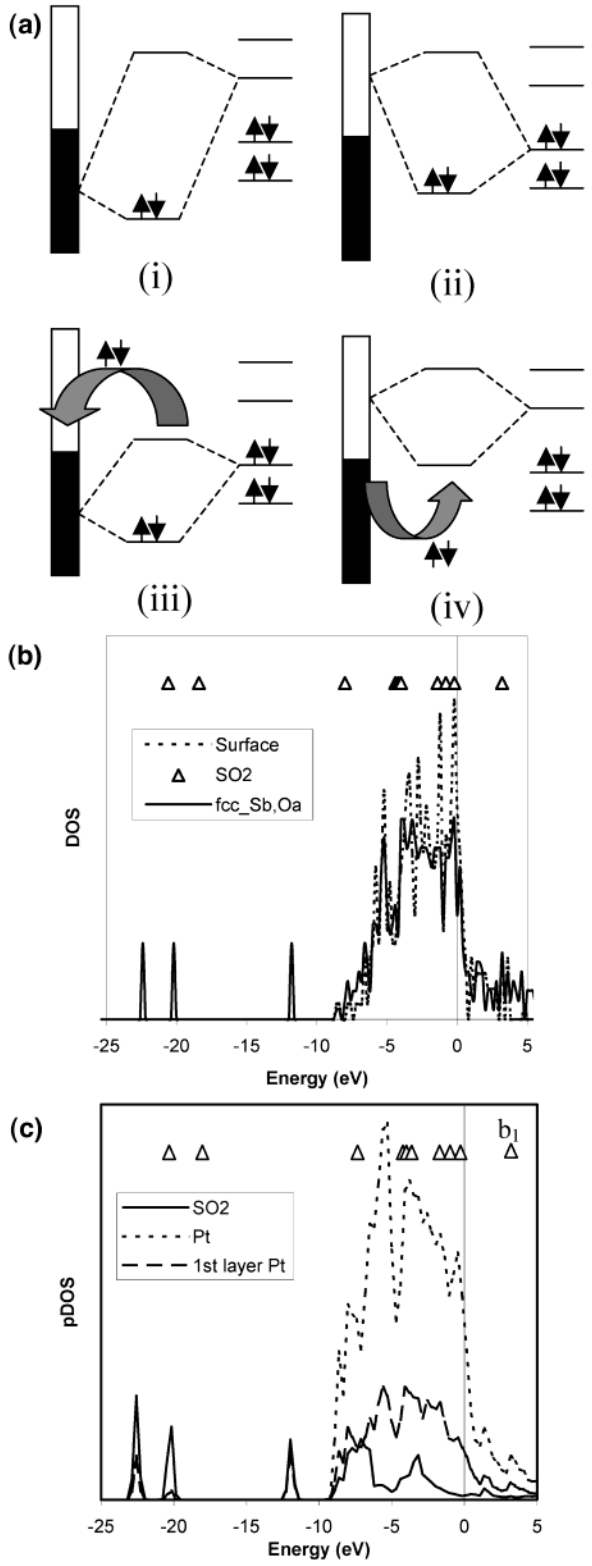

Figure 3. (a) Four types of orbital pair interactions occurring in the chemisorption process on metal surfaces. (b) Comparison of the DOS of gas-phase SO_2, the clean surface, and the most stable binding configuration fcc η^2-S_b,O_a. (c) Projected DOS of the fcc η^2-S_b,O_a configuration to its SO_2 component, the metal substrate component, and the topmost layer of the metal substrate component. The triangles mark the energy levels of gas-phase SO_2. All of the DOS are aligned by the corresponding Fermi levels.

the adsorbate, as shown in Figure 3a(i). This interaction effectively shifts electrons from the less electronegative species (metal) to the more electronegative species (adsorbate), driven by the difference of the electronic chemical potentials. Similarly, so-called back-donation is schematically shown in Figure 3a(ii). This involves the interaction of the unfilled bands of the metal with the occupied states of the adsorbate. Both of these effects, i.e., the charge forward donation and back-donation, occur in a large number of chemical reactions.[31] However, for chemical reactions on metal surfaces, two other unique bonding situations can occur. In one case, the occupied orbitals of the adsorbate interact with the filled bands of the substrate, transferring electrons from the antibonding orbitals to the Fermi level of the metal, as shown in Figure 3a(iii). In the other case, the unoccupied orbitals of the adsorbate interact with the unfilled bands of the substrate, transferring electrons from orbitals at the Fermi level to the bonding orbitals, as shown in Figure 3a(iv). These two additional binding situations extensively increase the pairing opportunities of the frontier orbitals and, thus, significantly enhance the energies of chemisorption of gas molecules on metal surfaces. Note that active d-bands in transition metals, such as the Pt surface in our case, can generally satisfy the overall symmetry requirement for appreciable orbital overlaps. All of these bonding effects essentially belong to the same class of orbital interactions, i.e., pairing of orbitals from both the substrate and the adsorbate to form bonding and antibonding molecular orbitals. These binding processes gain energy by occupying the bonding, but not the antibonding, orbitals. The only difference is in the origin and destination of the filling electrons. These are called first-order bonding events, the essential character of which is that orbitals end up with different energies after the bonding.[31]

An initial observation regarding these bonding situations is demonstrated in Figure 3b, which displays a direct comparison of the DOS of clean Pt(111) and fcc η^2-S_b,O_a, from which the induced DOS of this fcc η^2-S_b,O_a configuration can be obtained. As shown, the DOS of the active metal d-bands (at the Fermi level and down to -5 eV below) decreases dramatically upon binding. Through the interaction with the frontier orbitals of SO_2, a significant portion of the DOS is energetically stabilized through the creation of the bonding-type (the occupied bands with an energy of about -8 eV) and antibonding-type (the unoccupied bands with energy ~ 3 eV) orbitals.

By projecting the total wave function of fcc η^2-S_b,O_a onto the atomic basis sets of the adsorbate and substrate separately, one obtains the projected DOS shown in Figure 3c. One important feature of Figure 3c is the broadening of the six high-lying SO_2 orbitals in the metal d-band region below the Fermi level as a result of the bonding effects depicted in Figure 3a(ii) and 3a(iii). The second very important feature is that the LUMO level of the gas-phase SO_2 (termed b_1, which is the antibonding orbital at 3.0 eV consisting of three p orbitals perpendicular to the molecular plane, one from each atom) gets mixed into the extended metallic occupied d-bands and thus disappears almost entirely. (Compare the area of the residual b_1 peak to the area of broadened peaks in the metal d-band region.) The residual area of this b_1 peak is identified as the sulfur (Figure 4a) p (and some remaining d) orbitals (Figure 4b and 4c), which implies that most of the perpendicular p orbitals of both the oxygen atoms and the sulfur atom, consisting of the original b_1 orbital, have received electronic charge donations from the metal through the bonding events depicted in Figure 3a(i) and 3a(iv). It is also interesting to note the presence of resonance of the Pt substrate orbitals with the three low-lying SO_2 molecular orbitals (with the one-particle orbital energies -20.6, -18.4, and -8.0 eV of gas-phase SO_2), especially at the spike centered at the energy of -11.8 eV. These metal resonance components indicate

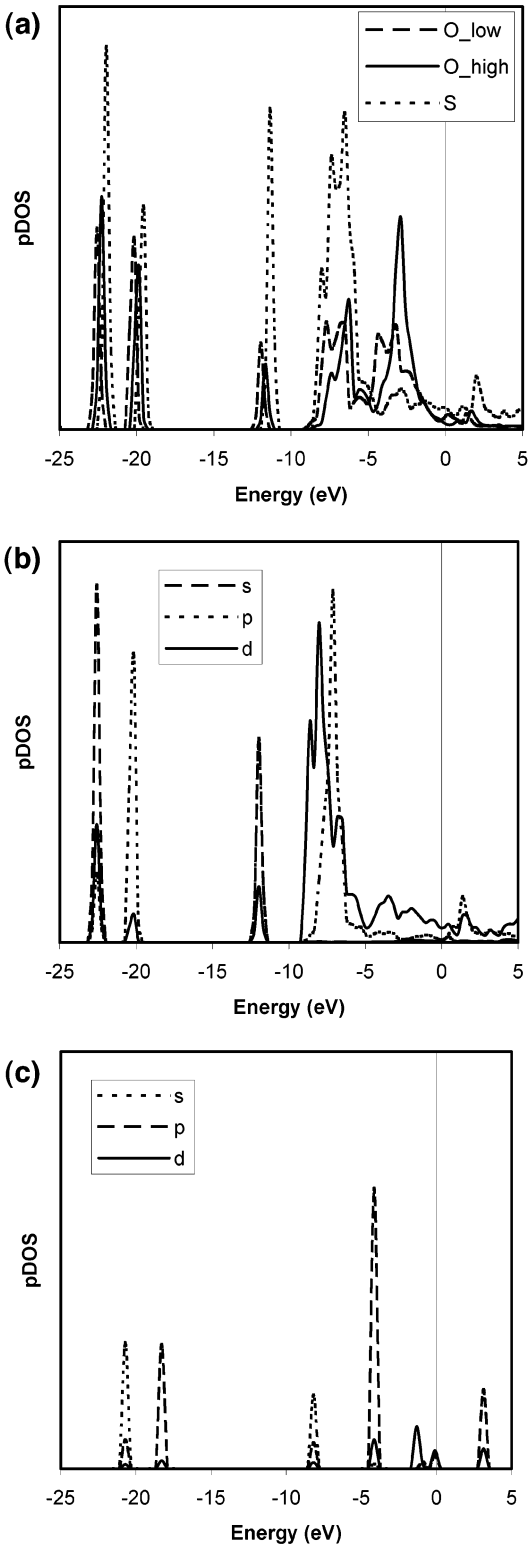

Figure 4. Projected DOS of the fcc η^2-S_b,O_a configuration to (a) the low-lying oxygen, the high-lying oxygen, and the sulfur atom components and (b) the s, p, and d components of the sulfur atom. (c) The pDOS of the isolated SO_2 to the s, p, and d components of its sulfur atom. All of the DOS are aligned by the corresponding Fermi levels.

the occurrence of back-donation of electronic charges. Both Figures 3c and 5a indicate that the chemical bonding of this type of orbital resonance in the charge back-donation event is essentially a local event, basically only involving the first-layer surface atoms of the Pt slab. Such a result helps to validate our use of a three-layer slab.

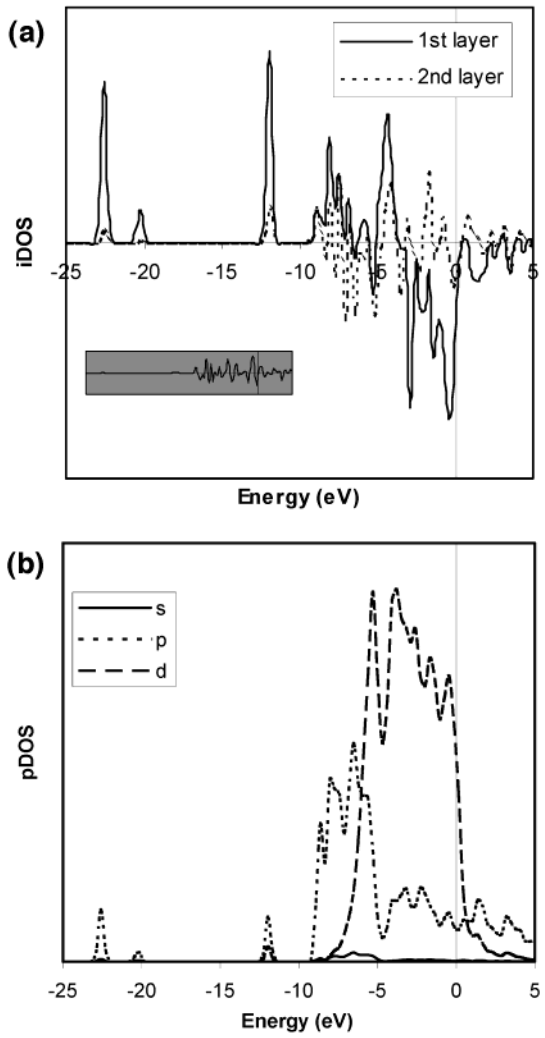

Figure 5. Substrate DOS of the fcc η^2-S_b,O_a configuration. (a) Induced DOS separated into the components by layers. Note that the iDOS of the third layer is shown as the inset. (b) Projected DOS to the s, p, and d components. All of the DOS are aligned by the corresponding Fermi levels.

Figure 3b also shows a clear downshift in energy of these three low-lying molecular orbitals, which indicates that the six high-lying occupied molecular orbitals in the metal d-band region have become more spatially diffuse. The fact that they are more diffuse leads to a decrease in screening of the low-lying orbitals by the high-lying ones and therefore a downshift in energy. By comparing the pDOS in Figure 4b and 4c, we can see that the d-character of the high-lying orbitals has increased upon adsorption and that this increase in d-character is consistent with the orbitals becoming more spatially diffuse.

Additionally, the so-called second-order bonding effects,[31] involving the bonding and antibonding in the bulk (not the atoms right on the uppermost surface), provide compensating effects to the direct change generated on the top of the surface by the adsorbates. One way of seeing this is by noticing the compensation in the DOS by the second-layer metal atoms to the first-layer ones (Figure 5a). There is no noticeable DOS compensation from the third layer, in which one observes a random oscillation pattern (inset of Figure 5a). This result helps to explain the small binding energy difference ($\sim$1$-$8 kJ/mol) that we observed between a four-layer slab and a three-layer slab.

The significance of sulfur in the SO_2 chemisorption is shown in Figure 4a, which identifies the sulfur atom as the major

contributor to the back-donation effect (especially for the spike at −11.8 eV). Specifically, as shown in Figure 4b, the primary contributions come from the sulfur 3s and 3p orbitals. Nevertheless, Figure 4b demonstrates the need to have the d-channels in the sulfur pseudopotential. They are responsible for the bonding to the d electrons of the metal (Figure 4b and 5b).

In summary, qualitatively good bonding requires a large broadening of the SO_2 frontier orbitals in the metal d-band region, a small unoccupied b_1 component left above the Fermi level, and a large resonance in the low-lying orbitals. Overall, the sulfur atom is the atom that contributes most to these orbital interactions. The second-order bonding effects provide an explanation to the question of why a three-layer Pt slab is a reasonably accurate model for SO_2 chemisorption on the Pt(111) surface.

Figure 6a shows that the flat-lying, strongly bound configuration fcc η^3-S_a,O_a,O_a stabilizes the bound SO_2 in a manner similar to that of the perpendicular configuration, fcc η^2-S_b,O_a (Figure 3c). The only difference is that the resonance at −11.4 eV is lower for η^3-S_a,O_a,O_a, which indicates that the back charge donation is decreased. Comparing the pDOS of fcc η^2-S_b,O_a (Figure 3c) with that of fcc η^3-S_a,O_b (Figure 6b), one sees that the pDOS in the filled metal d-band region (−10 eV to the Fermi level) of fcc η^2-S_b,O_a is broader than that of fcc η^2-S_a,O_b. The fact that the pDOS is broader in this region implies that there is more mixing between the orbitals of the adsorbate and those of the substrate, which in turn implies much stronger binding. From Table 1, it is clear that this is the case. Similar arguments can be made when comparing the pDOS of fcc η^2-S_b,O_a (Figure 3c) with that of bridge η^2-O,O || (Figure 6c). This gives a good explanation of our results on the small binding energies of the η^2-O,O configurations: an almost unoccupied b_1 still above the Fermi surface, little broadening of the orbitals in the metal d-band region, and little resonance of the low-lying orbitals.

C. Surface Coverage Effects, Dipole Moment, and Work Functions. Lateral adsorbate interactions on transition metal surfaces have a major effect on the adsorption and desorption kinetics, surface diffusion, and chemical reaction dynamics.[32,33] From a theoretical computational point of view, strong lateral interactions among adsorbate molecules can substantially affect the binding energetics computed by first-principles DFT calculations with plane-wave basis sets. It would certainly be desirable if one could estimate the energetics in the limit of infinitely small surface coverage based on the energetics of finite-sized supercells. In this section, we demonstrate this possibility in the case of SO_2 on the Pt(111) surface.

As shown in Table 1, SO_2 is bound more strongly to the Pt(111) surface as the surface coverage is lowered. From $^1/_4$ ML coverage to $^1/_9$ ML coverage, the binding energy increases by about 14−19 kJ/mol for the strongly bound and weakly bound configurations and by about 8 kJ/mol for the intermediately bound configurations. This implies the existence of strong repulsive interactions among the adsorbates. Because there is no net charge within any of the supercells in our study, the dominant term in the multipole expansion series is likely to be the dipole−dipole interaction term. Moreover, the fact that the interactions are repulsive further suggests that the dipole moment vectors have to be more perpendicular than parallel to the metal surface.

As expected, when the surface coverage is lower than some threshold, $^1/_4$ ML coverage in the case of SO_2 on Pt(111), the amplitude of the perpendicular surface dipole moment scales very nicely as $1/r^3$, where r is the physical separation of the first-neighbor adsorbates (refer to Figure 7a and Table 3). This indicates that the overall dipole moment has two main contributions: one is the dipole at infinite separation, namely, the permanent dipole, and the other is the induced dipole arising

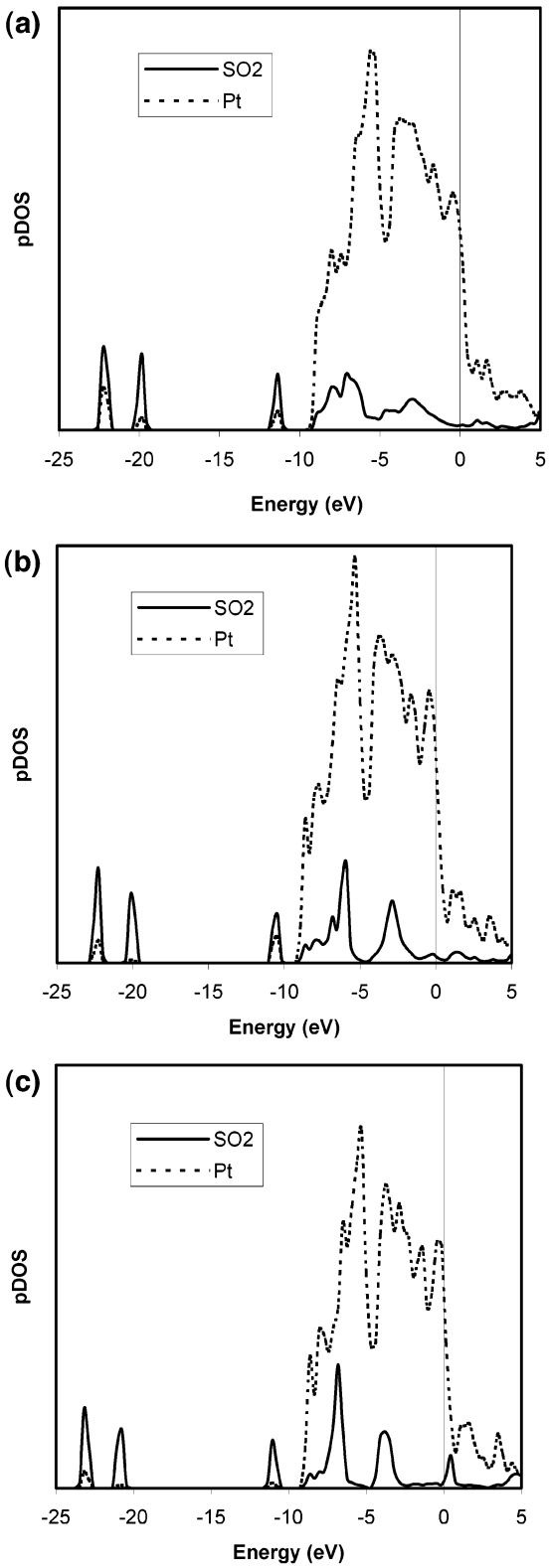

Figure 6. Projected density of states to the SO_2 component, the metal substrate component, and the topmost layer of the metal substrate component of three representative binding configurations: (a) fcc η^3-S_a,O_a,O_a (strong binding), (b) fcc η^2-S_a,O_b (intermediate binding), and (c) bridge η^2-O,O. (weak binding). All of the DOS are aligned by the corresponding Fermi levels.

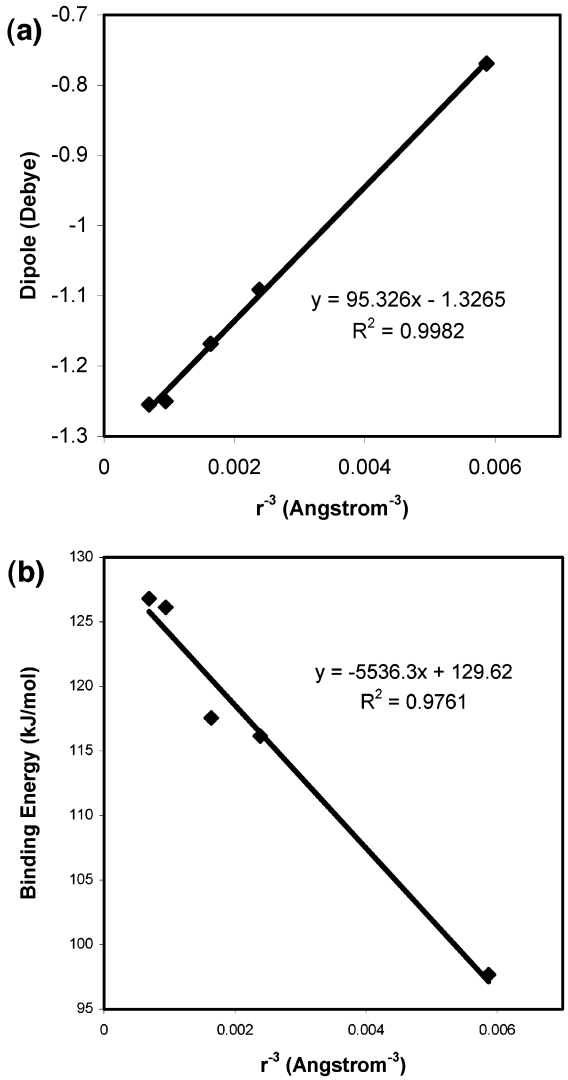

Figure 7. Correlation between (a) the *z* component of the dipole moment or (b) the binding energy and the distance between adsorbates to the −3 power. The intercept on the *y* axis in a gives an estimate of the permanent dipole moment, 1.33 D. The slope in b also estimates the permanent dipole moment, giving a value of 1.59 D. The intercept on the *y* axis in b can be used to estimate the binding energy at the limit of infinite separation of adsorbates, computed to be 129.6 kJ/mol.

from the electric field of neighboring dipoles

$$\mu = \mu_p + \mu_i = \mu_p\left(1 + \frac{\alpha}{r^3}\right).$$

The interaction energy of two parallel dipoles separated at a large distance is determined by the permanent dipoles

$$U = \frac{\mu^2}{r^3} \approx \frac{\mu_p^{\,2}}{r^3}, \qquad r \to \infty$$

This $1/r^3$ rule of the adsorbate interaction energy versus the adsorbate physical separation is demonstrated in Figure 7b. [Refer to Table 3 for detailed tabulated data. Note that the $(\sqrt{3} \times \sqrt{3})$R30° is not included in Figure 7b because it is below the distance threshold.] Figure 7b is important in the sense that it provides estimates of two important physical quantities at the zero coverage limit: the binding energy at infinite separation (the *y*-axis intercept) and the dipole moment at infinite separation (the slope). Assuming that the pairwise dipole interaction is only through the six first neighbors (which is certainly true when *r* approaches infinity, because the sum of the interaction energies of the infinite 2-D dipole lattice converges absolutely), the slope of Figure 7b reveals a value of 1.59 D for the permanent dipole moment, compared to the value of 1.33 D from the more direct estimation shown in Figure 7a. An adsorption energy of 129.6 kJ/mol is estimated at the low surface coverage limit. In summary, the most energetically stable molecularly adsorbed SO_2 configuration interacts mainly through a lateral dipole−dipole interaction on the Pt(111) surface. A similar conclusion was shown in the case of NH_3 on a 91-atom Pt cluster by Jennison et al. in their local density approximation DFT study.[34] Finally, one could apply this dipole−dipole interaction idea to explain the attractive interactions among adsorbates in cases where the dipole is more parallel, rather than perpendicular, to the metal surface.

Although repulsive interactions are quite significant among the SO_2 adsorbates, the relative energy differences among various binding configurations remain essentially unchanged. In particular, the strongest bound configuration, fcc η^2-S_b,O_a, remains the strongest bound configuration at a coverage of $^1/_9$ ML, as shown in Table 1. The overall molecular geometries of the adsorbate are almost identical under different surface coverages (Table 4). Only slight compression of the bonds on the order of a few hundredths of an angstrom is observed at lower surface coverages.

While observing the strong dipole−dipole interactions among molecularly adsorbed SO_2, one might wonder what the origin of this large dipole moment might be. Because of the high electronegativity of oxygen atoms, there is net negative charge transfer to the atomic oxygen when it binds to the clean Pt(111) surface. Rather surprisingly, atomic sulfur atoms bind to the Pt(111) surface through a very different scheme, producing a positive 0.4 D dipole moment on the surface (pointing from the substrate to the adsorbates), compared to −0.2 D for the atomic oxygen at $^1/_4$ and $^1/_9$ ML coverages on the Pt(111) surface. This was observed from experimental work function measurements on atomic sulfur on the Pt(111) surface.[35] In the case of molecularly adsorbed SO_2, the dipole moment is created by the difference in electronegativities between adsorbate sulfur and oxygen atoms. In general, the Pt−O bond length is substantially enlarged, ∼2.3 Å in the case of chemisorbed molecular fcc η^2-S_b,O_a compared to ∼2.0 Å in the case of the chemisorbed atomic fcc-O, which tends to increase the perpendicular dipole moment of the system. There is only a small perpendicular dipole moment in the flat-lying configurations,

TABLE 3: Lateral Interaction Effects on the Binding Energies of the fcc η^2-S_b,O_a Configuration on Pt(111) from $^1/_3$ ML to the Zero-Coverage Limit

surface coverage	$(\sqrt{3} \times \sqrt{3})$R30°	p(2 × 2)	$(\sqrt{7} \times \sqrt{7})$R19°	p(2 × 2)	$(\sqrt{13} \times \sqrt{13})$R14°	p(2 × 2)	zero limit (estimated)
binding energy (kJ/mol)	93.52	97.68	116.15	117.57	126.12	126.79	129.62
z-axis dipole moment (D)	−0.76	−0.77	−1.09	−1.17	−1.25	−1.25	−1.33

TABLE 4: Binding Geometry Changes of Pt(111)−p(3 × 3)−SO_2 with Respect to Pt(111)−p(2 × 2)−SO_2

	bond length increase (Å)		
configuration	S−O	Pt−S	Pt−O
	strong binding		
fcc η^2-S_b,O_a	0.00	0.00 (×2)	−0.04
	0.00		
hcp η^2-S_b,O_a	0.01	−0.02 (×2)	−0.10
	0.00		
bridge η^1-S ⊥	0.01	−0.01 (×2)	−0.05
	0.00		0.00
fcc η^3-S_a,O_a,O_a	0.01 (×2)	0.00	−0.03 (×2)
hcp η^3-S_a,O_a,O_a	0.01 (×2)	0.00	−0.03 (×2)
	intermediate binding		
atop η^3-S_a,O_b,O_b	−0.01 (×2)	−0.04	0.02, 0.03 (×2)
	weak binding		
bridge η^2-O, O.	0.03 (×2)		−0.39 (×2)

such as η^3-S_a,O_a,O_a; a very large perpendicular positive dipole moment in the η^2-O,O configurations; and an intermediate negative perpendicular dipole moment in the perpendicular and tilted sulfur-dominant binding configurations, such as η^2-S_a,O_b.

IV. Conclusions

We have performed a comprehensive series of DFT−GGA calculations on the chemisorption of SO_2 on Pt(111) slabs. Different binding groups were suggested to categorize binding trends among dozens of different binding configurations. The most strongly bound configuration was found to be fcc η^2-S_b,O_a with a binding energy of 97.7 at $^1/_4$ ML coverage. Dipole−dipole interactions are demonstrated to be responsible for the lateral repulsion among adsorbed SO_2 molecules at $^1/_4$ ML and lower surface coverages. Correlating the magnitude of these interactions as a function of distances between adsorbates leads us to estimate a binding energy of 129.6 kJ/mol at the zero surface coverage limit. Projected and induced density of states are used to interpret the underlying binding phenomena, including charge forward donation, back-donation, broadening of adsorbate frontier orbitals, and second-order compensating bonding of the bulk.

Acknowledgment. The authors thank Y. Yourdshahyan and A. M. Rappe for help with the pseudopotentials, C. A. Giurumescu and J. W. Chu for help in setting up the Beowulf cluster for the intensive computations, and R. Radhakrishnan for thoughtful discussions. This work was supported by Ford Motor Company and by an NSF grant under Contract CTS-9984301.

References and Notes

(1) Haase, J. *J. Phys.: Condens. Matter* **1997**, *9*, 3647.
(2) Rodriguez, J. A.; Hrbek, J. *Acc. Chem. Res.* **1999**, *32*, 719.
(3) Wilson, K.; Hardacre, C.; Baddeley, C. J.; Ludecke, J.; Woodfuff, D. P.; Lambert, R. M. *Surf. Sci.* **1997**, *372*, 279.
(4) Wilson, K.; Hardacre, C.; Lambert, R. M. *J. Phys. Chem.* **1995**, *99*, 13755.
(5) Lee, A. F.; Wilson, K.; Lambert, R. M.; Hubbard, C. P.; Hurley, R. G.; McCabe, R. W.; Gandhi, H. S. *J. Catal.* **1999**, *184*, 491.
(6) Lin, X.; Trout, B. L. Chemistry of Sulfur Oxides on Transition Metal Surfaces. In *Interfacial Applications in Environmental Engineering*; Keane, M., Ed.; Marcel Dekker: New York, 2003; p 55.
(7) Astegger, S.; Bechtold, E. *Surf. Sci.* **1982**, *122*, 491.
(8) Kohler, U.; Wassmuth, H.-W. *Surf. Sci.* **1982**, *126*, 448.
(9) Sun, Y. M.; Sloan, D.; Alberas, D. J.; Kovar, M.; Sun, Z. J.; White, J. M. *Surf. Sci.* **1994**, *319*, 34.
(10) Polcik, M.; Wilde, L.; Haase, J.; Brena, B.; Comelli, G.; Paolucci, G. *Surf. Sci.* **1997**, *381*, L568.
(11) Polcik, M.; Wilde, L.; Haase, J.; Brena, B.; Cocco, D.; Comelli, G.; Paolucci, G. *Phys. Rev. B* **1996**, *53*, 13720.
(12) Polcik, M.; Wilde, L.; Haase, J. *Phys. Rev. B* **1998**, *57*, 1868.
(13) Jackson, G. J.; Driver, S. M.; Woodruff, D. P.; Abrams, N.; Jones, R. G.; Butterfield, M. T.; Crapper, M. D.; Cowie, B. C. C.; Formoso, V. *Surf. Sci.* **2000**, *459*, 231.
(14) Rodriguez, J. A.; Ricart, J. M.; Clotet, A.; Illas, F. *J. Chem. Phys.* **2001**, *115*, 454.
(15) Yokoyama, T.; Terada, S.; Yagi, S.; Imanishi, A.; Takenaka, S.; Kitajima, Y.; Ohta, T. *Surf. Sci.* **1995**, *324*, 25.
(16) Terada, S.; Imanishi, A.; Yokoyama, T.; Takenaka, S.; Kitajima, Y.; Ohta, T. *Surf. Sci.* **1995**, *336*, 55.
(17) Zebisch, P.; Weinelt, M.; Steinruck, H.-P. *Surf. Sci.* **1993**, *295*, 295.
(18) Ku, R. C.; Wynblatt, P. *Appl. Surf. Sci.* **1981**, *8*, 250.
(19) Solomon, J. L.; Madix, R. J.; Wurth, W.; Stohr, J. *J. Phys. Chem.* **1991**, *95*, 3687.
(20) Berke, M. L.; Madix, R. J. *Surf. Sci.* **1988**, *194*, 223.
(21) Sellers, H.; Shustorovich, E. *Surf. Sci.* **1996**, *346*, 322.
(22) Sellers, H.; Shustorovich, E. *Surf. Sci.* **1996**, *356*, 209.
(23) See: http://www.fysik.dtu.dk/CAMP/dacapo.html.
(24) Neugebauer, J.; Scheffler, M. *Phys. Rev. B* **1992**, *46*, 16067.
(25) Makov, G.; Payne, M. C. *Phys. Rev. B* **1995**, *51*, 4014.
(26) Vanderbilt, D. *Phys. Rev. B* **1990**, *41*, 7892.
(27) Laasonen, K.; Pasquarello, A.; Car, R.; Lee, C.; Vanderbilt, D. *Phys. Rev. B* **1993**, *47*, 10142.
(28) Lin, X.; Ramer, N. J.; Rappe, A. M.; Hass, K. C.; Schneider, W. F.; Trout, B. L. *J. Phys. Chem. B* **2001**, *105*, 7739.
(29) Perdew, J. P.; Chevary, J. A.; Vosko, S. H.; Jackson, K. A.; Pederson, M. R.; Singh, D. J.; Fiolhais, C. *Phys. Rev. B* **1992**, *46*, 6671.
(30) Monkhorst, H. J.; Pack, J. D. *Phys. Rev. B* **1976**, *13*, 5188.
(31) Hoffmann, R. *Rev. Mod. Phys.* **1988**, *60*, 601.
(32) Einstein, T. L. In *Physical Structure of Solid Surfaces*; Unertl, W. N., Ed.; Elsevier: New York, 1996; Vol. 2.
(33) Kevan, S. D.; Skelton, D. C.; Wei, D.-H. *Crit. Rev. Surf. Chem.* **1994**, *3*, 77.
(34) Jennison, D. R.; Schultz, P. A.; Sears, M. P. *Phys. Rev. Lett.* **1996**, *77*, 4828.
(35) Billy, J.; Abon, M. *Surf. Sci.* **1984**, *146*, L525.